Communication

Vertically Polarized Compact Reconfigurable 360° Azimuth Scanning Array for Aviation Applications

Zhongyao Cao, Jiadong Hu, Yue Li, Kunpeng Wei, Zhijun Zhang, and Magdy F. Iskander

***Abstract*— In this communication, a 360° azimuth scanning array based on a compact reconfigurable element is proposed for aviation applications. In our design, a reconfigurable compact Yagi–Uda element is constructed by combing a driven element and two switchable parasitic elements. When constituting an array, more energy can be coupled to the parasitic elements and the current magnitude of the parasitic element reaches nearly the same as that of the driven element. Then, a tunable backside radiation zero point and high backside suppression can be realized for the Yagi–Uda element with only one reflector. The reconfigurable element is able to switch the radiation pattern between two broadside states in two directions and an endfire state. The measured results of the 1 × 8 prototype indicate that a wide scanning range from −180° to 180° is attained with a peak gain of 11.8 dBi and a gain fluctuation of less than 3 dB. The array has a small cross-sectional area of 0.47 × 0.26λ_0. This work provides a compact reconfigurable antenna with full 360° coverage for aviation applications. The tunable radiation zero point has the potential to promote future anti-interference array designs.**

***Index Terms*— 360° scanning, aviation applications, radiation zero point, reconfigurable element, wide-beamwidth element.**

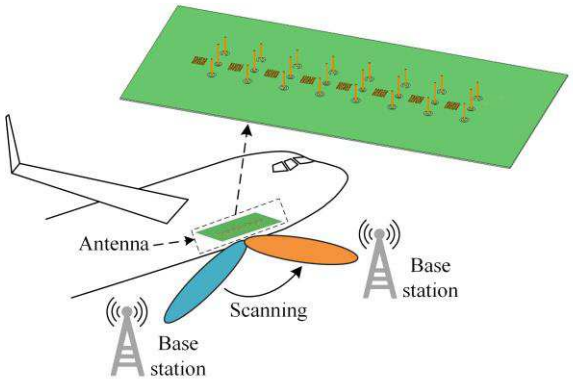

Fig. 1. Typical scenario of the proposed antenna in aviation applications.

I. Introduction

With the development of communication technology, the communication scene is increasingly expanding. The research on air-to-ground communication is of great significance in future applications. Fig. 1 shows the typical scenario in aviation applications. Generally, the distance between the aircraft and the base station is larger than 200 km, which means that the communication path is almost in the azimuth plane [1]. In addition, during the flight of the aircraft, the beam should have the ability of 360° coverage to link with the base stations that may appear in any direction. Considering the wind drag, a full 360° coverage antenna with a low cross-sectional area is desired.

Compact omnidirectional antennas are good candidates for aviation applications. Various compact omnidirectional antennas are studied in [2], [3], [4], [5], and [6] for space-limited scenarios. Omnidirectional patterns were obtained by using square column structures with magnetic dipoles [2], [3]. Instead of the square cavity structure, thin open cavities [4], [5] were proposed to decrease the cross-sectional area. Based on the aerodynamic analysis, a low wind drag wedge-profiled cavity was designed in [6]. Omnidirectional antennas have the merits of full azimuth coverage and low wind drag. However, in long-distance communications, high gain and high power are required to guarantee communication quality.

Circular arrays, which combine multiple high-gain antennas, have been widely studied with full azimuth coverage. Monopole antenna [7], [8], Alford loop with parasitic rings [9], and microstrip antenna with parasitic resonators [10] were proposed for multibeam full azimuth coverage but with large cross-sectional area. Lens antenna [11], [12] has the advantages of high gain and wide-angle operation, but with large widths, which makes it unsuitable for installation on the aircraft.

Instead of multibeam antennas, arrays with high gain and continuous scanning beams are alternatives to achieve wide-angle coverage. There are many designs focusing on widening the scanning range of the array [13], [14], [15], [16], [17], [18], [19], [20], [21]. Hollow cavity element [13] and backed cavity element [14], [15], [16] were designed and a scanning range from −60° to 60° was achieved. A novel magnetic dipole with wide beamwidths was proposed in [17] with an improved cover range from −76° to 76°. A wide-beam magnetoelectric dipole antenna was presented in [18] with wide coverage from −90° to 90°. To broaden the beamwidth of patch antennas, vertical metal walls were introduced in [19] and the scanning range of the array can be enhanced from −90° to 90°. Similarly, an artificial magnetic wall was added as the barrier plate to realize a half-space omnidirectional element pattern [20], but with a large space. In [1], two wide scanning monopole arrays were deployed back-to-back to achieve full 360° azimuth coverage. Back-to-back arrangement with double arrays improves the scanning range but increases the complexity, cost, and cross-sectional area.

The reconfigurable technique is also widely studied to improve the scanning range. In [21] and [22], a microstrip Yagi antenna element with switchable parasitic strips was proposed, which is able

Manuscript received 3 December 2022; revised 5 March 2023; accepted 20 March 2023. Date of publication 12 April 2023; date of current version 7 July 2023. This work was supported in part by the National Natural Science Foundation of China under Contract 61971254 and Contract 62271279. *(Corresponding author: Zhijun Zhang.)*

Zhongyao Cao, Yue Li, and Zhijun Zhang are with the Department of Electronic Engineering and the Beijing National Research Center for Information Science and Technology, Tsinghua University, Beijing 100084, China (e-mail: zjzh@tsinghua.edu.cn).

Jiadong Hu is with Huawei Technologies Company Ltd., Shanghai 201206, China.

Kunpeng Wei was with Honor Device Company Ltd., Beijing 100095, China. He is now with Xiaomi Communications Company Ltd., Beijing 100085, China.

Magdy F. Iskander is with the Hawaii Center for Advanced Communications, University of Hawai'i at Manoa, Honolulu, HI 96822 USA (e-mail: magdy.iskander@gmail.com).

Color versions of one or more figures in this communication are available at https://doi.org/10.1109/TAP.2023.3265459.

Digital Object Identifier 10.1109/TAP.2023.3265459

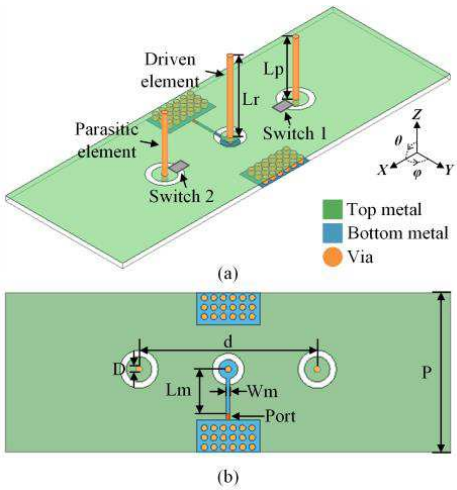

Fig. 2. Geometry of the array element. (a) Dimetric view. (b) Bottom view.

to switch or tune the radiation pattern and, thus, the beam can scan in a wide range. Two elements working at symmetrical modes in two subspaces were combined to scan its beam from $-81°$ to $81°$ [23]. A reconfigurable magnetic current element was proposed in [24]. By controlling the excitation of the adjacent magnetic elements, the half-plane from $-90°$ to $90°$ can be covered. However, achieving a reconfigurable array with full $360°$ coverage and a compact structure for aviation applications is still a challenge.

In this communication, a reconfigurable full $360°$ azimuth array is proposed with a small cross-sectional area and good backside suppression. The reconfigurable element consists of a driven element and two switchable parasitic elements. Different from a single Yagi–Uda antenna, when constructing an array, the Yagi–Uda element with only one reflector is enough to provide good suppression of backside radiation. The energy radiated backward from each driven element can be obtained by all the parasitic elements instead of the one just behind the excited element. The row of reflectors works as a whole periodic structure, which effectively blocks the backside radiation. Compared with the previous $360°$ scanning array, the proposed array has a smaller cross-sectional area of $0.47 \times 0.26\lambda_0$. The design is a good candidate for aviation applications. In addition, the tunable radiation zero point has the potential for future anti-interference designs.

II. Configuration and Design of the Array

A. Element Configuration

The proposed reconfigurable array element is shown in Fig. 2. The array element is designed based on two parasitic elements and a driven element. A metal ground is printed on the top layer of a 1-mm-thick FR-4 substrate ($\varepsilon_r = 4.4$ and $\tan\delta = 0.02$). The feeding structure is printed on the bottom layer of the substrate. A microstrip line with a width of 0.5 mm and a length of 8 mm is introduced for impedance matching. The metal ground is extended to the bottom layer by the metal vias to facilitate the implementation of the feed. The feeding microstrip line is connected to the driven element through the circular hole on the ground. Two switchable components, which can be p-i-n diodes or micro-electro-mechanical systems (MEMS) switches, are added to the parasitic elements to realize beam switching. The parasitic elements can be connected to the ground to form a reflector or disconnected from the ground to form a suspended element by switching. The detailed parameters of the array element are shown in Table I.

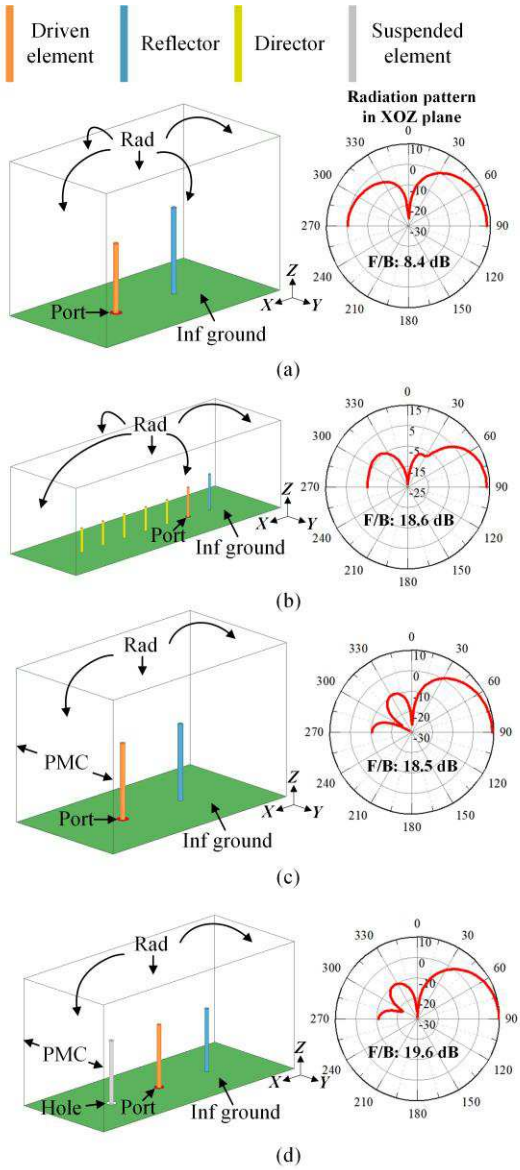

Fig. 3. Radiation patterns of different Yagi–Uda antennas in the XOZ plane. (a) One reflector and (b) one reflector and five directors in free space. (c) One reflector and (d) one reflector and one suspended element in ideal array environment.

B. Operating Principle

To realize wide-angle scanning, a good front-to-back (F/B) ratio of the element is required. Fig. 3 presents four different Yagi–Uda antennas with different radiation boundaries. For the Yagi–Uda antenna with only one reflector in Fig. 3(a), a limited F/B of 8.4 dB is obtained. Traditionally, to improve the F/B and gain, directors are introduced in front of the radiation element. An improvement in F/B of about 10 dB can be observed for the Yagi–Uda antenna with five directors and one reflector, as shown in Fig. 3(b). As shown in Fig. 3(c), a good F/B of 18.5 dB can also be achieved with only one reflector. In the simulation, perfect magnetic conductor (PMC) boundaries are used to approximate the radiation pattern of the array when all the elements are excited in phase, that is to say, constructing an array is another way to enhance the F/B and gain of Yagi–Uda antennas. The suppression of backside radiation is guaranteed by the backside zero point formed in the array environment. Finally, when a suspended element is introduced in Fig. 3(d), the radiation

TABLE I
DETAILED DIMENSIONS OF THE PROPOSED ARRAY ELEMENT

Parameter	Value (mm)	Parameter	Value (mm)
Lp	11.8	Wm	0.5
Lr	15	Lm	7
d	28	P	26
D	1		

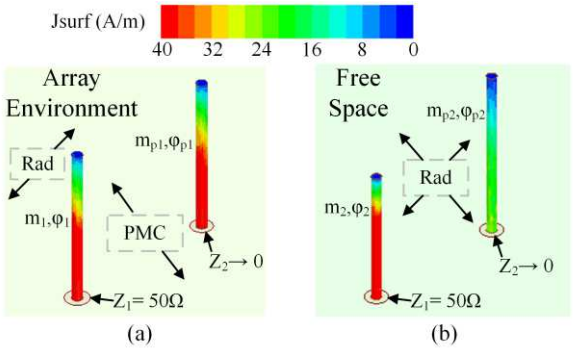

Fig. 4. Simulated complex magnitude current distributions of Yagi–Uda antenna with one reflector in (a) array environment and (b) free space.

performance keeps nearly the same as that of the antenna in Fig. 3(c). The reason for this phenomenon is that a suspended element cannot reach the resonant length and has little effect on the radiation pattern. Therefore, a reconfigurable element with a directional radiation pattern can be achieved.

To explain the generation of the zero point, we analyze the current distribution of the driven element and the reflector. According to the mutual impedance relationship between two elements, the voltage on both ports can be expressed as [25]

$$U_1 = I_1 Z_{11} + I_2 Z_{12} \tag{1}$$

$$0 = I_1 Z_{21} + I_2 Z_{22} \tag{2}$$

where U_1 and I_1 are the voltage and current on the driven element, respectively, I_2 is the current on the reflector, and Z_{ij} is the self-impedance or mutual impedance of the elements. The ratio of the current on the passive element and the radiation element can be obtained from (2)

$$\frac{I_2}{I_1} = -\frac{Z_{21}}{Z_{22}} == \frac{m_2 e^{j\varphi_2}}{m_1 e^{j\varphi_1}} \tag{3}$$

$$\frac{m_2}{m_1} = \left| -\frac{R_{12} + jX_{12}}{R_{22} + jX_{22}} \right| = \sqrt{\frac{R_{12}^2 + X_{12}^2}{R_{22}^2 + X_{22}^2}} \tag{4}$$

$$\varphi_2 - \varphi_1 = \arctan\left(\frac{R_{22}X_{12} - R_{12}X_{22}}{R_{12}R_{22} + X_{12}X_{22}}\right) \tag{5}$$

where m_i is the magnitude of the current, φ_i is the phase of the current, R_{ij} is the real part of Z_{ij}, and X_{ij} is the imaginary part of Z_{ij}.

Fig. 4 presents the complex magnitude current distributions in the array environment and free space. The port impedance of the reflector is set to a value approaching zero to approximate the short circuit. Then, the impedance matrix can be obtained and the current magnitude ratio can be calculated by (3). As shown in Fig. 5(b), the phase difference between the elements at 5 GHz is the same in both conditions. However, the current magnitude of the reflector in the array environment is remarkably higher than that in free space, as shown in Fig. 4(a) and (b). The current magnitude of the reflector is enhanced to almost the same as that of the driven element, as

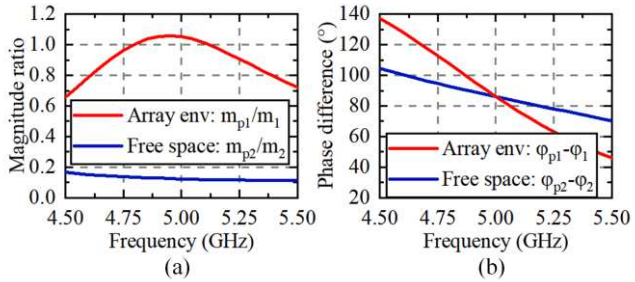

Fig. 5. Simulated (a) magnitude ratio and (b) phase difference between the reflector and driven element in different radiation environment.

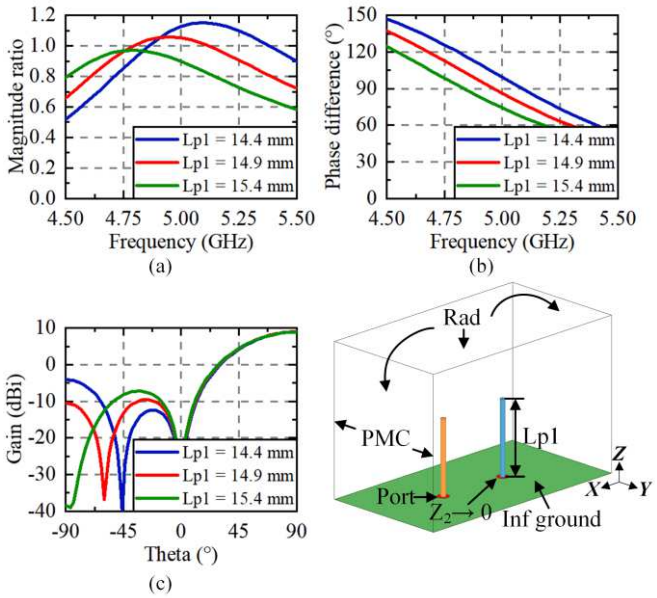

Fig. 6. Simulated (a) magnitude ratio and (b) phase difference between the reflector and driven element. (c) Radiation pattern in XOZ plane in ideal array environment.

shown in Fig. 5(a). Good suppression of backside radiation can be realized for the Yagi–Uda antenna with only one reflector when constructing an array. The reason for this phenomenon is that the parasitic elements in an array are not working independently but form a 1-D periodic structure and stop the wave from propagating backward. The backside energy radiated from each driven element is obtained and blocked by all the parasitic elements in the array. The superimposing of the induced current from all the driven elements and the coupling between the parasitic elements result in the improvement of the current magnitude of the parasitic elements.

Besides, the zero point can be steered by changing the height of the reflector Lp1. The operating frequency of the design is at the resonant frequency of the parasitic element. As shown in Fig. 6(a), when Lp1 decreases to 14.4 mm, more energy will be coupled to the parasitic element and the magnitude ratio will be higher than one. However, the current magnitude on both elements keeps comparable. As shown in Fig. 6(b), when varying Lp1, the phase difference can be managed. Thus, by changing Lp1 from 14.4 to 15.4 mm with a 0.5-mm step, the angle of the zero point can be steered from −46° to −85°, as presented in Fig. 6(c). The tunable zero point has the potential for dynamic interference suppression in future designs with the use of varactors, which can realize electrical height tuning of the parasitic elements.

C. Array Design and Scanning Strategy

Based on the properties analyzed above, a reconfigurable Yagi–Uda antenna array is proposed. A uniform linear 1 × 8 array is designed with a ground size of 120 × 270 mm. Each array element consists of a

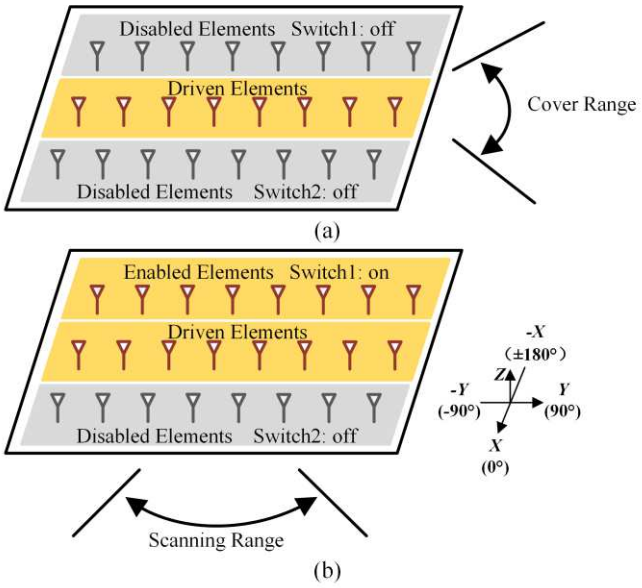

Fig. 7. Two kinds of azimuth plane scanning states of the proposed 1 × 8 reconfigurable array. (a) Endfire state. (b) Broadside state.

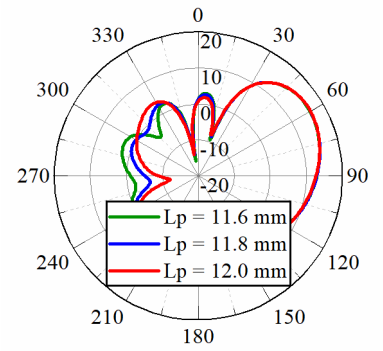

Fig. 8. Simulated radiation pattern of the 1 × 8 array on the finite ground in broadside state in E-plane with different lengths Lp of parasitic element.

driven element and two switchable parasitic elements. In the endfire state, a unidirectional pattern is required. To avoid grating lobe in the endfire state, the distance between elements should be lower than 0.5 λ_0. We compromise between the gain and suppression level of the grating lobe. In our design, the distance between the elements is set as 25 mm (0.41 λ_0).

To clearly illustrate the operating principle of the array in the scanning process, the beam coverage and states of the switches are presented in Fig. 7. For the endfire scanning state, all the switches are turned off for better impedance matching. For the broadside scanning state, a row of switches in the array are turned on. Then, a row of reflectors can be generated on one side of the driven elements. The broadside scanning state and endfire scanning state are combined to cover the full 360° azimuth plane. The coverage under different switch states is summarized in Table II. Under two broadside scanning states, the beam can cover the range from −70° to 70° and from 110° to −110°. When scanning to larger angles, the gain of the broadside state drops rapidly. Therefore, for large-angle coverage, an endfire state with all the switches turned off is introduced to maintain a high gain. Both in the broadside state and endfire state, the array is excited with a specific phase distribution. The phase difference $\Delta\varphi$ between the adjacent element in different beam angles is summarized in Table III.

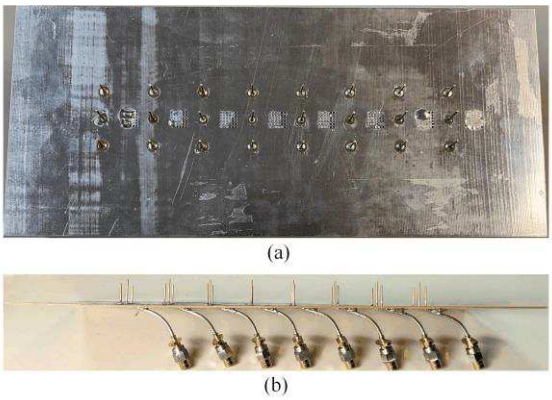

Fig. 9. Fabricated prototype of the proposed array. (a) Top view. (b) Side view.

TABLE II
ANGLE COVERAGE UNDER DIFFERENT SWITCH STATES

Scanning states	Switch 1	Switch 2	Coverage
Broadside 1	On	Off	-70°~70°
Broadside 2	Off	On	110°~180°; -180°~-110°
Endfire	Off	Off	-90°; 90°

TABLE III
ANGLE COVERAGE UNDER DIFFERENT BEAM ANGLES AT 5 GHz

$\Delta\varphi$	Ang	Gain[1] (dBi)	Gain[2] (dBi)			SLL (dB)		
			Sim.[3]	Sim.[4]	Mea.	Sim.[3]	Sim.[4]	Mea.
0°	0°	14.7	12.0	11.5	11.3	13.5	13.1	9.4
52°	20°	14.4	11.7	11.2	11.4	12.4	12.4	10.3
99°	40°	13.8	10.9	10.5	10.7	11.7	11.8	9.1
133°	60°	13.0	10.2	9.9	9.7	10.7	10.6	7.5
148°	70°	12.5	9.9	9.6	9.0	9.8	9.7	6.0
158°	90°	12.6	10.1	10.1	10.1	13.2	13.2	12.4

1: On the infinite ground. 2: On the finite ground. 3: Using ideal switches. 4: Using non-ideal switches

The simulated radiation patterns in the E-plane on the finite ground with different lengths of parasitic elements are shown in Fig. 8. The backside zero point can also be observed in the 1 × 8 array on the finite ground. The depth of the zero point deteriorates due to the scatter of the truncated ground. However, backside radiation suppression can still be observed. In the design, we set Lp as 11.8 mm. Generally, as a reflector, the parasitic element is higher than the driven element. However, the height relationship is reversed in the proposed array. It can be attributed to the feeding structure of the driven element. Circular slots are cut on the ground to provide space for the elements. The equivalent reactance loading effect of the slots increases the resonant frequency of the driven elements.

III. PROTOTYPE AND MEASUREMENT OF THE PROPOSED ARRAY

To validate the performances of the proposed array, a 1 × 8 array with a ground size of 120 × 270 mm is fabricated, as shown in Fig. 9. Semirigid cables are utilized to feed the elements and all the elements are made of copper. For quick verification of the performance of the array, metal plates were used to equivalent the effect of switches. Two versions of the array were fabricated to validate the radiation performance under the broadside state and the endfire state.

As demonstrated in [20], when scanning to the endfire direction, the problem of active impedance mismatch of the array inevitably arises. In the endfire state, the energy radiated by each element propagates along the direction of the array extension. The energy

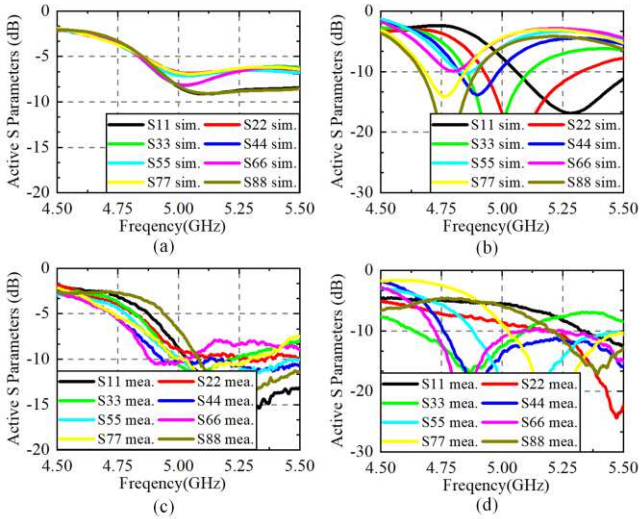

Fig. 10. Simulated and measured S parameters in different scanning states. (a) Broadside state (simulated). (b) Endfire state (simulated). (c) Broadside state (measured). (d) Endfire state (measured).

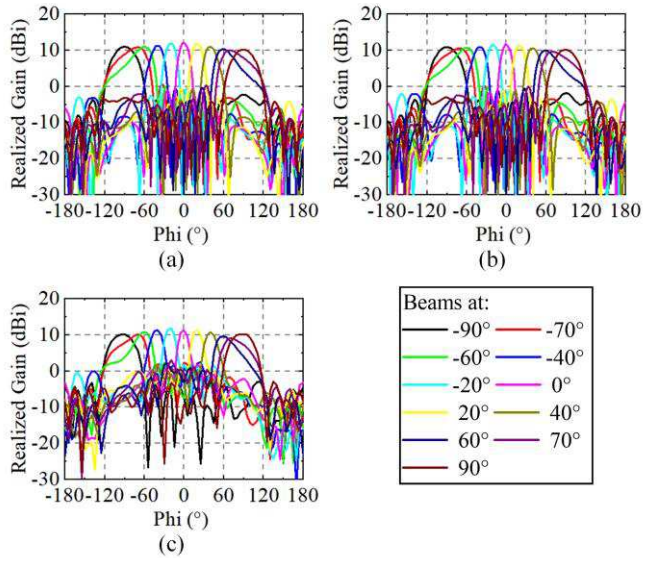

Fig. 11. Scanning performance at 5 GHz in the H-plane of the proposed antenna array. (a) Simulated results with ideal switches. (b) Simulated results with nonideal switches. (c) Measured results.

coupled from the phase-leading elements is superimposed in the same phase and seriously deteriorates the active impedance matching of the phase-lagging elements. However, the directivity of the endfire state is still sufficient to provide a high gain to cover the endfire direction. Fig. 10 shows the simulated and measured active S parameters under the broadside state and endfire state. In the measurement, the influence of the semirigid cable feeding line is deembedded. The microstrip line is designed to obtain good impedance matching in the endfire state. Then, a low gain fluctuation can be realized during scanning. In the measurement, except for the testing ports, 50-Ω loads are connected to other ports. Then, the active S parameters of the elements can be calculated according to the phase relationship in different scanning states based on the analysis in [26].

To verify the performance of the array with actual switches, the equivalent circuits of the switches are considered in the simulation. The typical OFF-state capacitance (=30 fF) and ON-state resistance (=1 Ω) of the MEMS switch are modeled as an impedance boundary [27]. The scanning performance at 5 GHz in the H-plane is shown in Fig. 11. Due to the symmetry of the array, the beam scanning

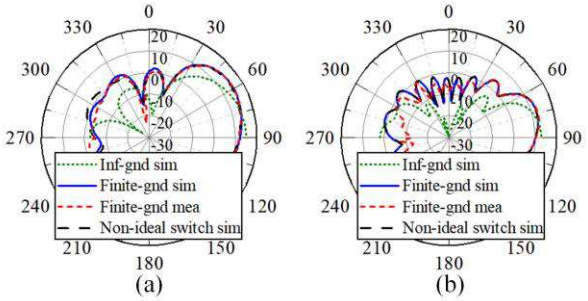

Fig. 12. Scanning performance at 5 GHz in the E-plane of the proposed antenna array. (a) Broadside state (at 0°). (b) Endfire state (at 90°).

range from −90° to 90° is depicted to illustrate the full azimuth scanning ability of the array for brevity. The simulated patterns with ideal and nonideal switches are similar in shape. The detailed performance of the array is summarized in Table III. The simulated maximum and minimum gains of 12.0 and 9.9 dBi are, respectively, realized with ideal switches in the azimuthal plane. With nonideal switches used, the maximum gain drops to 11.5 dBi and the efficiency drops from 0.82 to 0.74 at 5 GHz due to the loss introduced by the ON-state resistance. The equivalent capacitance of the switch on the parasitic elements has a negligible effect on the proposed array. Therefore, in the endfire state with all switches in the OFF-state, the gain and efficiency are the same as that of the ideal switches. In the measurement, the active radiation patterns of the elements are utilized to synthesize the radiation patterns of the array in different beam angles [26]. The measured maximum and minimum gains are 11.8 and 9.0 dBi, respectively. The measured gain fluctuation is less than 3 dB. Affected by the fabrication error, the measured maximum gain appears at −20°. In general, the measured results accord well with the simulated results.

The scanning performance at 5 GHz in the E-plane is shown in Fig. 12. When deploying on the finite ground, because of the truncation effect, the beam tilts to 60° in the elevation plane. The measured gain of the broadside state and endfire state in the elevation plane is 15.1 and 12.6 dBi, respectively. The angle of the zero point also tilts from −60° to −50° with the finite ground. Due to the scatter on the edge of the truncated ground, the cancellation of backside radiation is weakened and the depth of the zero point deteriorates. However, good backside radiation suppression can still be achieved in the proposed array with only one reflector. The radiation patterns with nonideal or ideal switches show almost the same performance. Thus, the reconfigurable array is feasible using actual switches in a real electronic environment.

Table IV summarizes the performance of this work and other wide-angle scanning arrays. The designs in [18], [21], and [24] are only able to realize half-plane coverage. Thus, for 360° coverage in aviation applications, two arrays are demanded, which complicates the design and increases the cost. By combining high gain antenna elements to a circular array [8], full 360° coverage is achieved but with a large cross-sectional area of $3.74 \times 0.32\lambda_0$ (λ_0 is the wavelength at the center frequency point). In [1], two wide-angle monopole arrays are placed back-to-back to broaden the beam coverage. Although the array can cover the range of 360°, the back-to-back design uses twice the number of elements, which requires more transmitter and receiver (T/R) components and a large cross-sectional area of $0.7 \times 0.32\lambda_0$. In this design, the element number and cross-sectional area are reduced by utilizing the good backside radiation suppression property of the Yagi–Uda antenna in the array environment. Compared to the array in [1], the cross-sectional area of the proposed array is reduced to 54.6% and the element number is reduced to 50% while maintaining other performance comparable.

TABLE IV
COMPARISON AMONG THE WIDE-ANGLE SCANNING ARRAY

Reference	Type	Beam coverage range	Cross section area (λ_0^2)	Number of units	Gain (dBi) Broadside; Endfire
[1]	Monopole Array	-180°~180°	0.70 × 0.32	16	10.8; 8.8
[8]	Multi-beam Circular Array	-180°~180°	3.74 × 0.32	18	12.5; 12.5
[18]	Magnetoelectric dipole Array	-90°~90°	0.11 × 0.50	12	10.3; 9.1
[21]	Reconfigurable Array	-87°~87°	0.15 × 0.41	5	8.9; 3.4
[24]	Reconfigurable Array	-90°~90°	0.25 × 1.35	8	15.5 ;12.8
This work	Reconfigurable Array	-180°~180°	0.47 × 0.26	8	11.3; 10.1

The proposed array has the merits of a small cross-sectional area and low complexity with full 360° coverage, which is suitable for aviation applications.

IV. CONCLUSION

In this communication, a 360° full azimuth scanning array is proposed with a compact structure and a tunable radiation zero point. A reconfigurable Yagi–Uda antenna element is designed with two parasitic switchable reflectors. In the array environment, the current magnitude of the parasitic element reaches the same level as that of the driven element. Then, backside radiation is well suppressed by only one reflector and a compact array element with two switchable reflectors is constructed. The measured results show that the proposed array realizes a full 360° scanning with a peak gain of 11.8 dBi, a gain fluctuation of less than 3 dB, and a small cross-sectional area of $0.47 \times 0.26\ \lambda_0$. The array is a good candidate for aviation applications. In addition, the tunable backside zero point has the potential to promote anti-interference array designs.

REFERENCES

[1] J. Hu, Y. Li, and Z. Zhang, "Vertically polarized 360° azimuth scanning array," *IEEE Antennas Wireless Propag. Lett.*, vol. 21, no. 5, pp. 898–902, May 2022.

[2] Y. Li, Z. Zhang, J. Zheng, and Z. Feng, "Design of dual-polarized monopole-slot antenna with small volume and high isolation," *IEEE Trans. Antennas Propag.*, vol. 60, no. 5, pp. 2511–2514, May 2012.

[3] Y. Li, Z. Zhang, J. Zheng, and Z. Feng, "Compact azimuthal omnidirectional dual-polarized antenna using highly isolated colocated slots," *IEEE Trans. Antennas Propag.*, vol. 60, no. 9, pp. 4037–4045, Sep. 2012.

[4] P. Liu, Y. Li, Z. Zhang, and Z. Feng, "Omnidirectional dual-polarized antenna with sabre-like structure," *IEEE Trans. Antennas Propag.*, vol. 65, no. 6, pp. 3221–3225, Jun. 2017.

[5] P. Liu, Z. Meng, L. Wang, Y. Zhang, and Y. Li, "Omnidirectional dual-polarized saber antenna with low wind drag," *IEEE Trans. Antennas Propag.*, vol. 68, no. 1, pp. 558–563, Jan. 2020.

[6] Y. Zhang, P. Liu, Y. Yin, and Y. Li, "Omnidirectional dual-polarized antenna using co-located slots with wedgy profile," *IEEE Trans. Antennas Propag.*, vol. 69, no. 9, pp. 5446–5454, Sep. 2021.

[7] T. Zhang, S.-Y. Yao, and Y. Wang, "Design of radiation-pattern-reconfigurable antenna with four beams," *IEEE Antennas Wireless Propag. Lett.*, vol. 14, pp. 183–186, 2015.

[8] Y. Wen, P.-Y. Qin, G.-M. Wei, and R. W. Ziolkowski, "Circular array of endfire Yagi–Uda monopoles with a full 360° azimuthal beam scanning," *IEEE Trans. Antennas Propag.*, vol. 70, no. 7, pp. 6042–6047, Jul. 2022.

[9] Y. Zhang, Z. Han, S. Tang, S. Shen, C.-Y. Chiu, and R. Murch, "A highly pattern-reconfigurable planar antenna with 360° single- and multi-beam steering," *IEEE Trans. Antennas Propag.*, vol. 70, no. 8, pp. 6490–6504, Aug. 2022.

[10] Y. Zhang et al., "A low-profile microstrip vertically polarized endfire antenna with 360° beam-scanning and high beam-shaping capability," *IEEE Trans. Antennas Propag.*, vol. 70, no. 9, pp. 7691–7702, Sep. 2022.

[11] T. M. Nguyen, T. K. Vo Dai, and O. Kilic, "Design of a 360° scanning circularly symmetric polygon lens," *IEEE Trans. Antennas Propag.*, vol. 66, no. 9, pp. 4458–4465, Sep. 2018.

[12] J. Li et al., "Design of a broadband metasurface Luneburg lens for full-angle operation," *IEEE Trans. Antennas Propag.*, vol. 67, no. 4, pp. 2442–2451, Apr. 2019.

[13] Z.-F. Ding, X. Shaoqiu, C. Liu, M.-C. Tang, C. Zhang, and B.-Z. Wang, "Design of a broadband, wide-beam hollow cavity multilayer antenna for phased array applications," *IEEE Antennas Wireless Propag. Lett.*, vol. 15, pp. 1040–1043, 2016.

[14] H. Liu, A. Qing, Z. Xu, Z. Yu, and S. Zhang, "Design of physically connected wideband SIW cavity-backed patch antenna for wide-angle scanning phased arrays," *IEEE Antennas Wireless Propag. Lett.*, vol. 20, no. 3, pp. 406–410, Mar. 2021.

[15] R. L. Xia, S. W. Qu, S. Yang, and Y. Chen, "Wideband wide-scanning phased array with connected backed cavities and parasitic striplines," *IEEE Trans. Antennas Propag.*, vol. 56, no. 4, pp. 1767–1775, Apr. 2018.

[16] F.-L. Jin, W. Shao, L.-Y. Xiao, B.-Z. Wang, and B. Jiang, "Substrate-integrated cavity-backed array with controlled mutual coupling for wide scanning," *IEEE Antennas Wireless Propag. Lett.*, vol. 21, no. 4, pp. 808–812, Apr. 2022.

[17] C.-M. Liu, S.-Q. Xiao, H.-L. Tu, and Z. Ding, "Wide-angle scanning low profile phased array antenna based on a novel magnetic dipole," *IEEE Trans. Antennas Propag.*, vol. 65, no. 3, pp. 1151–1162, Mar. 2017.

[18] H. Yang, X. Cao, J. Gao, H. Yang, and T. Li, "A wide-beam antenna for wide-angle scanning linear phased arrays," *IEEE Antennas Wireless Propag. Lett.*, vol. 19, no. 12, pp. 2122–2126, Dec. 2020.

[19] G. Yang, Q. Chen, J. Li, S. Zhou, and Z. Xing, "Improving wide-angle scanning performance of phased array antenna by dielectric sheet," *IEEE Access*, vol. 7, pp. 71897–71906, 2019.

[20] R. Wang, B.-Z. Wang, X. Ding, and X.-S. Yang, "Planar phased array with wide-angle scanning performance based on image theory," *IEEE Trans. Antennas Propag.*, vol. 63, no. 9, pp. 3908–3917, Sep. 2015.

[21] S. Xiao, C. Zheng, M. Li, J. Xiong, and B.-Z. Wang, "Varactor-loaded pattern reconfigurable array for wide-angle scanning with low gain fluctuation," *IEEE Trans. Antennas Propag.*, vol. 63, no. 5, pp. 2364–2369, May 2015.

[22] Y.-Y. Bai, S. Xiao, M.-C. Tang, Z.-F. Ding, and B.-Z. Wang, "Wide-angle scanning phased array with pattern reconfigurable elements," *IEEE Trans. Antennas Propag.*, vol. 59, no. 11, pp. 4071–4076, Nov. 2011.

[23] Y.-F. Cheng, X. Ding, W. Shao, M.-X. Yu, and B.-Z. Wang, "A novel wide-angle scanning phased array based on dual-mode pattern-reconfigurable elements," *IEEE Antennas Wireless Propag. Lett.*, vol. 16, pp. 396–399, 2017.

[24] X. Ding, Y.-F. Cheng, W. Shao, H. Li, B.-Z. Wang, and D. E. Anagnostou, "A wide-angle scanning planar phased array with pattern reconfigurable magnetic current element," *IEEE Trans. Antennas Propag.*, vol. 65, no. 3, pp. 1434–1439, Mar. 2017.

[25] C. A. Balanis, *Antenna Theory Analysis and Design*, 3rd ed. Hoboken, NJ, USA: Wiley, 2005.

[26] D. M. Pozar, "A relation between the active input impedance and the active element pattern of a phased array," *IEEE Trans. Antennas Propag.*, vol. 51, no. 9, pp. 2486–2489, Sep. 2003.

[27] A. Zohur, H. Mopidevi, D. Rodrigo, M. Unlu, L. Jofre, and B. A. Cetiner, "RF MEMS reconfigurable two-band antenna," *IEEE Antennas Wireless Propag. Lett.*, vol. 12, pp. 72–75, 2013.